Earth and Planetary Science Letters 305 (2011) 290–296

Contents lists available at ScienceDirect

Earth and Planetary Science Letters

journal homepage: www.elsevier.com/locate/epsl

Principal earthquakes: Theory and observations from the 2008 West Bohemia swarm

Václav Vavryčuk

Institute of Geophysics, Academy of Sciences, Boční II/1401, 141 00 Praha 4, Czech Republic

ARTICLE INFO

Article history:
Received 16 November 2010
Received in revised form 28 February 2011
Accepted 3 March 2011
Available online 7 April 2011

Editor: P. Shearer

Keywords:
earthquake
failure criterion
fault friction
focal mechanism
tectonic stress

ABSTRACT

Earthquakes that occur on optimally oriented fault planes with respect to the tectonic stress regime display two distinct focal mechanisms and are fundamental characteristics of each seismically active region. These earthquakes, which we term 'principal', need not coincide with the strongest earthquakes or need not occur along the major active faults in the region. Stability analysis of diversely oriented fault planes under a given stress reveals that the focal mechanisms connected with unstable fault planes should not be very distinct from those of the principal earthquakes. The P/T axes form clusters with a typical two-wing or 'butterfly' pattern. This pattern is particularly visible when constructing the failure curves defined as a projection of the Mohr–Coulomb failure criterion in the Mohr's diagram onto the focal sphere. The position, shape and size of the failure curves depend on the stress orientation, shape ratio, friction and on the size of the instability area in the Mohr's diagram.

The theoretical analysis is tested using accurately determined focal mechanisms of 99 micro-earthquakes that occurred during the 2008 earthquake swarm in the West Bohemia/Vogtland region. The distribution of P/T axes reveals the butterfly wing pattern predicted in numerical modelling. The activated fault planes concentrate in the area of validity of the Mohr–Coulomb failure criterion. The average friction of faults is 0.5 and corresponds to a deviation of 32° of the principal faults from the σ_1 axis. The left-lateral strike-slip principal fault was the most active fault during the swarm. It shows little geological expression at the surface but it is clearly defined by a linear cluster of hypocentres at depth. The right-lateral strike-slip principal fault was less active but it is geologically well manifested on the Earth's surface.

1. Introduction

The analysis of traction on faults generated by tectonic stress in a seismically active area is essential for understanding the occurrence of earthquakes and seismicity (Scholtz, 2002). Traction on a fault basically depends on the orientation of the fault with respect to the local stress field. This can be graphically represented using the Mohr's circle diagram (Jaeger and Cook, 1979; Mavko et al., 2009). All possible combinations of effective normal traction and shear traction generated by tectonic stress on an arbitrary oriented fault plane fill the area between the large and small circles in the diagram (Fig. 1). This area is subdivided into areas of stable (shadow area) and unstable (red area) fault planes using the Mohr–Coulomb failure criterion (Beeler et al., 2000; Scholtz, 2002; Zoback, 2010). If shear traction is higher than the critical value τ_c, calculated from cohesion C, friction μ on a fault, normal traction σ_n, and pore pressure p:

$$\tau > \tau_c = C + \mu(\sigma_n - p), \tag{1}$$

the fault becomes unstable, and an earthquake along this fault can occur. The larger the area in the Mohr's diagram delimited by the failure criterion (Fig. 1, red area), the higher the variety in orientations of unstable fault planes. Consequently, the variety of fault orientations projects into a variety of admissible focal mechanisms of earthquakes. This provides the possibility of studying the failure criterion from seismic observations (Iio, 1997). Given a large set of well-determined focal mechanisms in a seismically active area, we can study a variety of orientations of active faults and their clustering in the Mohr's circle diagram. Subsequently, we can infer an appropriate failure criterion valid for the studied region.

In this paper, we analyze the statistical properties of focal mechanisms with respect to tectonic stress and failure conditions using numerical modelling as well as observations. In numerical modelling, we study theoretical distributions of nodal lines and P/T axes for various stress and failure conditions and for various levels of errors of focal mechanisms. We show that an essential role is played by fault planes optimally oriented with respect to the stress (Fig. 1, blue dot). To emphasize their significance, we call them 'principal faults'. Consequently, we use the terms 'principal earthquakes' and 'principal focal mechanisms' for earthquakes and mechanisms associated with the principal faults. We study properties of the principal focal mechanisms and their relation to fault friction and tectonic stress. Finally, the theoretical analysis is tested using accurately determined focal mechanisms of 99 micro-earthquakes that occurred during the 2008 earthquake swarm in the West Bohemia/Vogtland region, Czech Republic.

E-mail address: vv@ig.cas.cz.

0012-821X/$ – see front matter © 2011 Elsevier B.V. All rights reserved.
doi:10.1016/j.epsl.2011.03.002

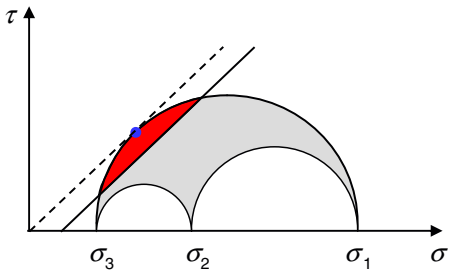

Fig. 1. Mohr's circle diagram. Points satisfying the Mohr–Coulomb failure criterion lie within the area marked in red colour. The blue dot marks the position of the optimally oriented fault plane. The dashed line is parallel to the Mohr–Coulomb failure criterion and tangent to the Mohr's circles. σ and τ are the effective normal traction and the shear traction, respectively. σ_1, σ_2 and σ_3 are the principal stresses.

2. Numerical modelling

The variety in orientations of unstable fault planes can be studied under different stress regimes by numerical modelling. In modelling, we assume the tectonic stress to be homogeneous, and cohesion C, friction μ and pore pressure p in Eq. (1) to be constant. We generate randomly distributed fault planes within the unstable area of the Mohr's diagram and study the focal mechanisms expected for earthquakes occurring along these fault planes. The orientation of the slip on the fault is assumed to be in the direction of shear traction projected into the fault plane (Gephart and Forsyth, 1984; Michael, 1984). The left-hand plot of Fig. 2a shows the Mohr's diagram, the failure criterion and the positions of randomly distributed unstable fault planes. The middle and right-hand plots of Fig. 2a show the nodal lines and the P/T axes for corresponding focal mechanisms in the lower-hemisphere equal-area projection. The nodal lines and P/T axes of the focal mechanisms associated with randomly generated fault planes inform us about the predominant type of faulting and about the scatter in orientations of the unstable faults. The P and T axes form clusters of a specific shape and size (Fig. 2a, right-hand plot). The form of the clusters is best demonstrated using the 'failure curves' defined as the projection of the Mohr–Coulomb failure criterion (Fig. 2b, left-hand plot) onto the focal sphere (Fig. 2b, right-hand plot). Since the Mohr's circle diagram is usually shown only in one half-plane, but both half-planes must be considered when generating the failure curves, the failure criterion splits into two closed curves for the P axes as well as for the T axes on the focal sphere. The two P/T failure curves may intersect each other or be separated. The area inside the failure curves define positions of the P/T axes of focal mechanisms conceivable under the given stress regime.

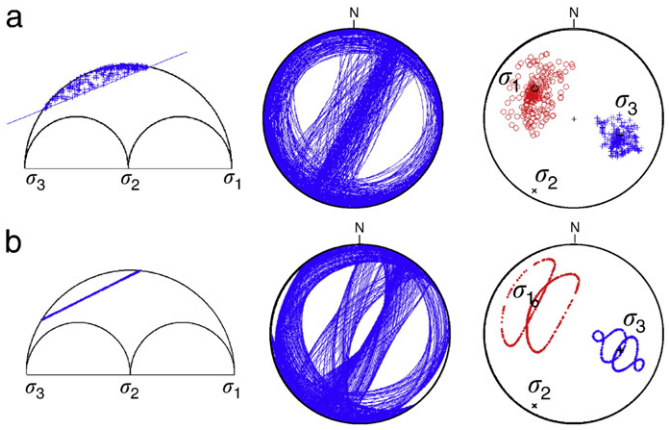

Fig. 2. Statistical properties of focal mechanisms associated with unstable fault planes. (a) Randomly distributed fault planes inside the unstable area of the Mohr's diagram (left), corresponding nodal lines (in the middle), and the P/T axes (right). The P axes are marked by red circles, the T axes by blue crosses. (b) Fault planes lying on the Mohr–Coulomb failure line (left, blue line), corresponding nodal lines (in the middle), and the P/T axes (right). The P/T axes form the P (red)/T (blue) fracture curves displaying the two-wing butterfly pattern. The directions (azimuth/plunge) of the σ_1, σ_2 and σ_3 stress axes are: 308°/44°, 209°/9° and 110°/44°. The shape ratio R is 0.5. The azimuth is measured clockwise from the north, and the plunge from the horizontal plane. Friction μ in the Mohr-Coulomb failure criterion is 0.5.

The modelling shows that the failure curves are sensitive to friction μ on faults (Fig. 3a and b), to pore pressure p (Fig. 3c and d) and to shape ratio R, $R=(\sigma_1-\sigma_2)/(\sigma_1-\sigma_3)$. Very often, the P/T axes do not form just one cluster but two sub-clusters, the split failure curves being not overlapped but separated. We call this effect the 'two-wing pattern' or the 'butterfly wings'. The butterfly wings are separated well, if friction is high (Fig. 3b). If friction is low, the wings come closer or they overlap. A similar effect is also observed, if pore pressure increases. In this case, the distance between the centres of the butterfly wings remains constant, but enlarging the area of unstable fault planes (compare Fig. 3c and d) causes the wings to become larger so that they may eventually touch or overlap. With real data, it can also happen that the two-wing pattern is hidden owing to inaccuracies in the focal mechanisms. For example, focal mechanisms retrieved with an error of 20° in strike, dip and rake can smear the distribution of the P/T axes so significantly that the original two-wing pattern is no longer identifiable (Fig. 4c).

3. Principal focal mechanisms

The fault planes satisfying the failure criterion have various probabilities of being activated. This probability can be roughly measured by the instability of the fault defined as

$$I=\frac{\tau-\tau_c}{\tau_c}. \tag{2}$$

The higher the instability, the higher the probability of the fault being activated. Obviously, a prominent fault plane is the plane optimally oriented in the stress field having thus the highest instability and being most susceptible to failure (Fig. 1). This plane and the earthquake occurring along this plane are called 'principal'. Each stress allows for the existence of at least two distinct principal fault planes and two distinct principal focal mechanisms (Fig. 5). The reason for the existence of two principal mechanisms is the same as for observing the two-wing pattern of the failure curves. The P/T axes of the principal focal mechanisms lie within the two P/T butterfly wings. If pore pressure is decreased, the wings become smaller being shrunk to the P/T axes of the principal focal mechanisms in the limit.

The orientation of the principal fault planes and principal focal mechanisms depends on stress and fault friction. The B axes of both principal focal mechanisms coincide with the σ_2 axis (Fig. 5b). The P/T axes lie in the σ_1–σ_3 plane: the σ_1 axis is in the centre between the two P axes, and the σ_3 axis is in the centre between the two T axes. The principal fault planes are those nodal planes whose deviation from the σ_1 axis is less than 45°. Deviation θ between the two principal fault planes and the σ_1 axis is expressed by a formula similar to that for the 2-D stress: $\theta=0.5\arctan\mu^{-1}$. Since the relation between the principal focal mechanisms and the orientation of stress is simple, the inversion for stress from principal focal mechanisms is straightforward. On the other hand, we cannot retrieve the shape ratio from the principal focal mechanisms. The difficulty of determining the shape ratio is inherent in all stress inversions (Angelier, 2002; Gephart and Forsyth, 1984; Lund and Slunga, 1999; Michael, 1984), because its determination is data demanding. The shape ratio constrains the mutual relation between the size and shape of the P and T butterfly wings. Therefore, a rather large set of focal mechanisms is needed to map the wings accurately.

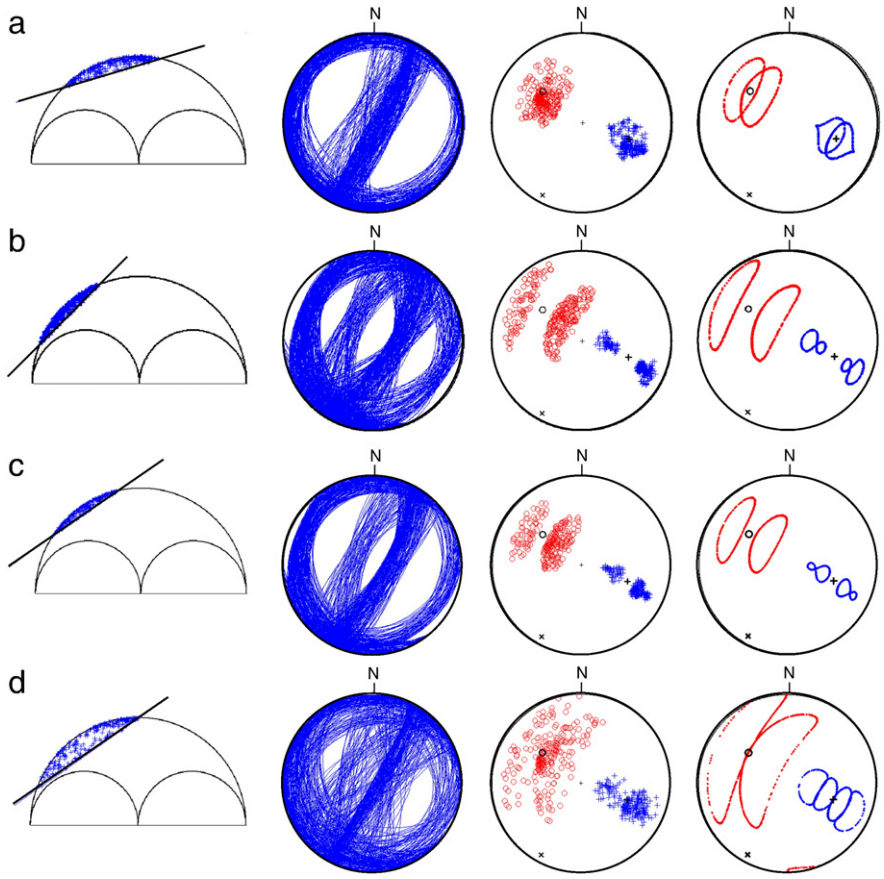

Fig. 3. Mohr's diagrams, nodal lines, P/T axes and failure curves under various stress conditions. (a) Low friction ($\mu=0.3$), (b) high friction ($\mu=1.0$), (c) low pore pressure, and (d) high pore pressure. The friction in (c) and (d) is 0.7. The orientation of stress axes and the shape ratio are the same as in Fig. 2.

4. Application to the West Bohemia earthquake swarm in 2008

4.1. West Bohemia/Vogtland region

The significance of principal earthquakes and principal focal mechanisms is demonstrated on the seismicity in the West Bohemia/Vogtland region, the border area between the Czech Republic and Germany. The area is typical for the occurrence of earthquake swarms. The seismic activity is probably connected to young Quaternary volcanism manifested by numerous springs of mineral water with a high content of carbon dioxide. One of the strongest recent earthquake swarms occurred in October 2008 (Fischer et al., 2010). This swarm lasted for four weeks and involved about 25.000 micro-earthquakes with

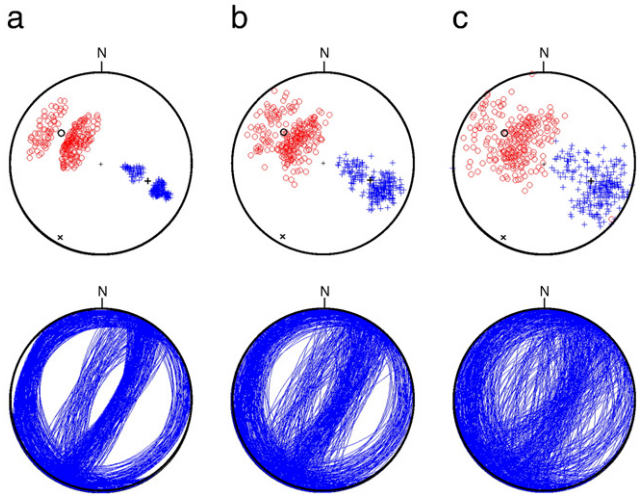

Fig. 4. Scatter of the P/T axes (upper plots) and nodal lines (lower plots) in dependence on the accuracy of focal mechanisms. The strike, dip and rake of the focal mechanisms (a) are contaminated by random noise with uniformly distributed error up to 10° (b) and 20° (c). For parameters of stress, see Fig. 3c.

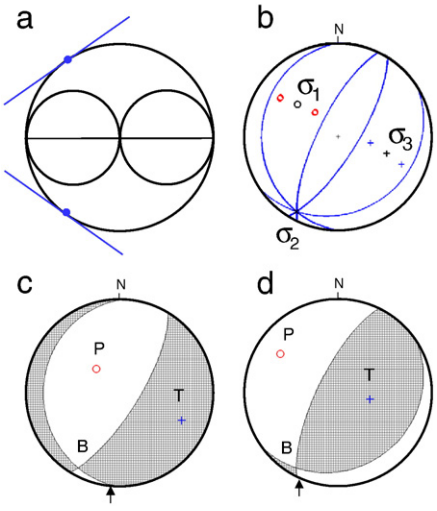

Fig. 5. Principal focal mechanisms. (a) Full Mohr's circle diagram, (b) principal nodal lines and P/T axes, and (c) and (d) principal focal mechanisms. The blue dots in (a) mark the positions of the principal fault planes. The arrows in (c) and (d) identify the principal fault planes. The strike, dip and rake of the principal focal mechanisms are: $\phi_1=181°$, $\delta_1=20°$, $\lambda_1=-119°$, and $\phi_2=206°$, $\delta_2=72°$, $\lambda_2=80°$. $R=0.5$ and $\mu=0.7$. Lower-hemisphere equal-area projection is used.

magnitude greater than −0.5. The largest event had a magnitude 3.8. The epicentres formed a 4 km long cluster striking N170°E. The hypocentres were located at depths of 7.5–10 km. The tectonic structure of the area is characterized by two main fault systems (Babuška et al., 2007): the Sudeten NW–SE fault system and the Ore-Mountain (Eger Rift) WSW–ENE fault system. The NW–SE fault system is considered as a continuation of the Mariánské Lázně fault. Tectonic complexity of the area is manifested by existence of other minor fault systems (Bankwitz et al., 2003).

4.2. Data

The 2008 swarm was recorded by 22 three-component short-period seismic West Bohemia Network (WEBNET) stations (Fig. 6a) surrounding the swarm epicentres (Fischer et al., 2010). The sampling frequency was 250 Hz and the frequency band was flat from 0.5 to 60 Hz. Since the micro-earthquakes were recorded by many stations with excellent focal sphere coverage (Fig. 6b and c), the data provide a unique opportunity of retrieving the focal mechanisms and tectonic stress in this area very accurately. The procedure was as follows. First, focal mechanisms of about 450 micro-earthquakes were calculated using the inversion of P-wave amplitudes. We selected 167 micro-earthquakes of this data set by discarding those with identical or very similar focal mechanisms in order to cover homogeneously a whole variety of mechanisms which occurred during the swarm. We then applied the waveform inversion to increase the accuracy of the focal mechanisms. In the inversion, we used the records of the vertical component of the direct P wave with a duration of 0.2–0.4 s depending on the magnitude of the event. The Green functions were calculated using the ray method (Červený, 2001) and incorporated the effects of the Earth's surface. The full moment tensors (MT) were calculated using the generalized linear inversion and decomposed into the double-couple (DC) and non-double-couple (non-DC) components (Vavryčuk, 2002). The reliability of the MT was assessed by calculating the root-mean-square difference (RMS) between the synthetic and observed waveforms and by the variance reduction. Based on the RMS and variance reduction, we selected 99 micro-earthquakes with the most accurate focal mechanisms. The accuracy of the focal mechanisms or moment tensors can be quantified using various approaches (Hardebeck and Shearer, 2002; Šílený, 2009). Here, the accuracy was quantified by repeating inversions using randomly generated noisy input data with noise level of 20%, biased hypocentres with a mislocation of 250 m in the epicentre and 500 m in depth, and models of varying structure with velocity perturbations of 5%. From these tests we estimated the standard errors in the strike, dip and rake angles to be less than 3°.

Finally, we inverted the set of the 99 most accurate focal mechanisms for principal stress directions and for the shape ratio using the Angelier inversion (Angelier, 2002), see Fig. 7. This method is a modification of the Gephart and Forsyth (1984) method and it is based on maximizing the slip shear stress component (SSSC). The

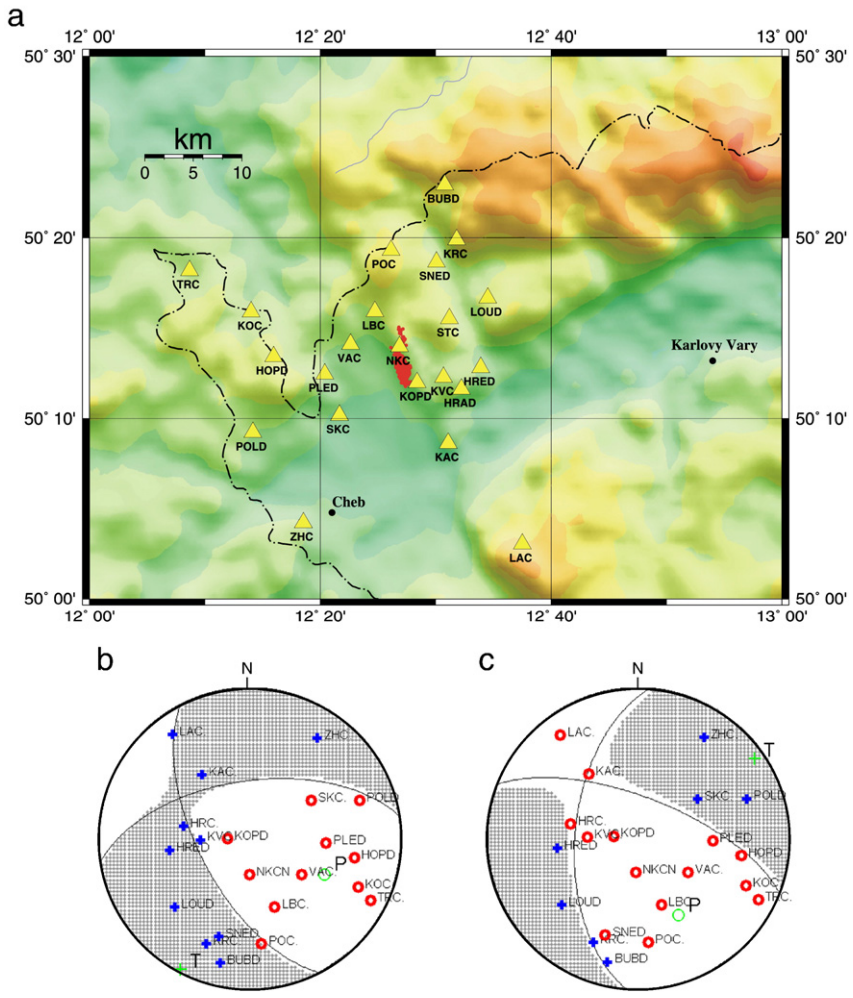

Fig. 6. (a) Topographic map of the West/Bohemia/Vogtland region. The epicentres of the 2008 swarm micro-earthquakes are marked by red dots, the WEBNET stations are marked by yellow triangles. (b) Focal mechanism of the $M_L = 1.4$ event (Oct 6, 2008, 03:39:29 UTC). (c) Focal mechanism of the $M_L = 0.8$ event (Oct 6, 2008, 09:21:13 UTC). Red circles and blue crosses in (b) and (c) denote the minus and plus polarities of the P waves, respectively. The hatched area does not match the nodal lines exactly, because the full moment tensors are slightly non-double-couple. Lower-hemisphere equal-area projection is used.

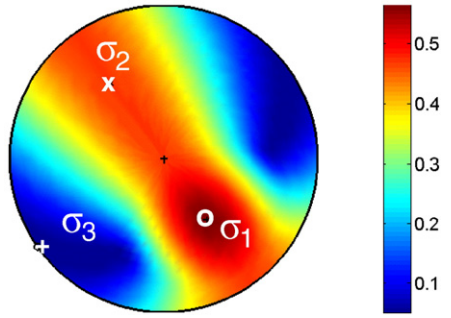

Fig. 7. Inversion for stress using the method of Angelier (Angelier, 2002). The mean value of the slip shear stress component (SSSC) over all input focal mechanisms is shown in colour as a function of the σ_1 direction. The optimum σ_1 direction is in the maximum of the SSSC. The lower-hemisphere equal-area projection is used. The directions of the σ_1, σ_2 and σ_3 axes are (azimuth/plunge): 146°/48°, 327°/42° and 237°/1°. The shape ratio R is 0.55. The black plus sign marks the vertical direction.

method avoids the necessity to identify the fault plane with one of the two nodal planes of each focal mechanism in the inversion. The SSSC function is maximized using the robust grid search inversion scheme. The approach recovers four parameters of the stress tensor: three angles defining the directions of the three principal stresses, σ_1, σ_2 and σ_3, and shape ratio R, $R=(\sigma_1-\sigma_2)/(\sigma_1-\sigma_3)$. The inversion for the optimum stress tensor was performed using a 1° grid in searching through the principal stress directions and a 0.05 increment in searching for R.

4.3. Results

The results of the stress inversion yield a N146°E direction for the maximum compressive principal stress (see Fig. 7), which coincides well with the average direction N144°E in Western Europe (Heidbach et al., 2008; Müller et al., 1992). The value is slightly rotated with respect to N160°E measured at the KTB superdeep borehole (Brudy et al., 1997), located about 50 km SW of the West Bohemia region. Interestingly, the σ_3 axis is horizontal but the σ_1 and σ_2 axes deviate from the horizontal by about 45°. The shape ratio R is 0.55.

Knowing the stress field we can plot the Mohr's diagram together with the positions of the active fault planes (Fig. 8a). In contrast to numerical modelling, when focal mechanisms were uniquely inferred from the orientation of fault planes and from stress, the identification of fault planes from focal mechanisms is ambiguous. To solve this difficulty, we follow Lund and Slunga (1999) and identify the fault plane of each mechanism with the nodal plane of higher instability I, see Eq. (2). As a result, Fig. 8a shows a compact clustering of activated fault planes in the Mohr's diagram (left-hand plot) in the area where we assume the Mohr–Coulomb failure criterion to be valid. Moreover, a butterfly wing pattern is clearly visible in the distribution of the P/T axes (Fig. 8a, right-hand plot). This indicates a high accuracy of the focal mechanisms (compare Figs. 4 and 8a) and homogeneity of the retrieved stress. Either inaccurate focal mechanisms or inhomogeneous stress field should smear the butterfly wings.

By modelling synthetic focal mechanisms we can adjust the shape ratio which is an unstable parameter in the stress inversion. Comparing the theoretical and observed nodal lines and P/T axes in Fig. 8a and b we can see that the shapes of the butterfly wings are slightly different. In order to adjust the butterfly wings better, we refine the shape ratio to be 0.8. Fig. 8c and d show a good match between the real and synthetic data. From the distribution of fault planes in the Mohr's diagram (Fig. 8c) we construct empirically the Mohr–Coulomb failure criterion and determine the average friction to be 0.50 ± 0.05. Consequently, the deviation of the principal faults from the σ_1 axis is 32° and the two conjugate principal focal mechanisms are defined by the following angles: $\phi_1=169°$, $\delta_1=68°$, $\lambda_1=-44°$, and $\phi_2=304°$, $\delta_2=66°$, $\lambda_2=-137°$ with an error of $\pm1°$. Note that

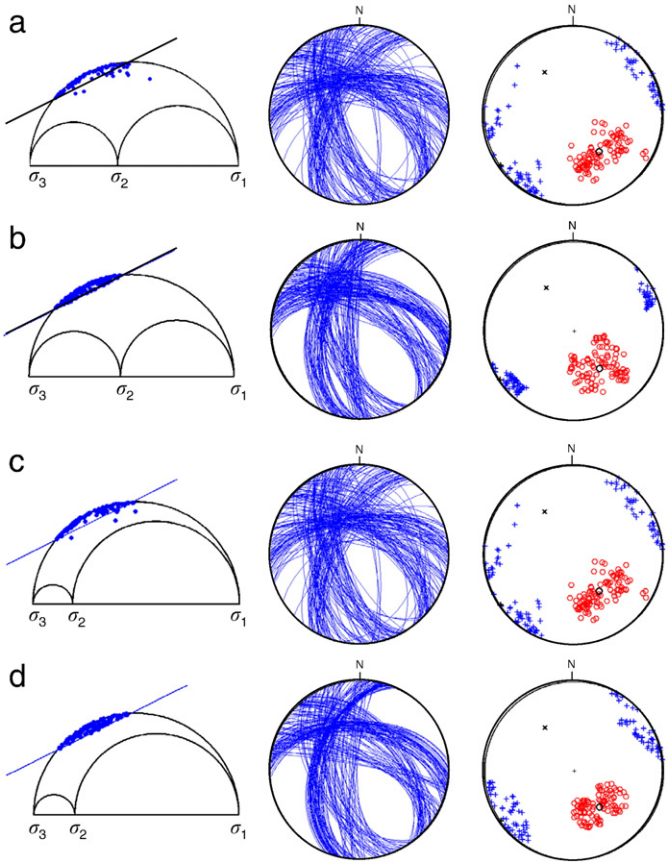

Fig. 8. Mohr's diagrams, nodal lines and the P/T axes for the observed (a and c) and synthetic (b and d) data. The shape ratio is 0.55 in (a) and (b). The shape ratio was refined to 0.80 in (c) and (d) by comparing the distributions of the observed and synthetic P/T axes and finding their best match. The optimum value of friction is 0.50.

friction of 0.5 is slightly less than the value 0.6–0.8 predicted from laboratory measurements (Byerlee, 1978) or the prevailing value 0.6 observed under geological conditions (Scholtz, 2002).

If we inspect the clustering of active faults in the Mohr's diagram for the two conjugate fault systems separately, we can even study the

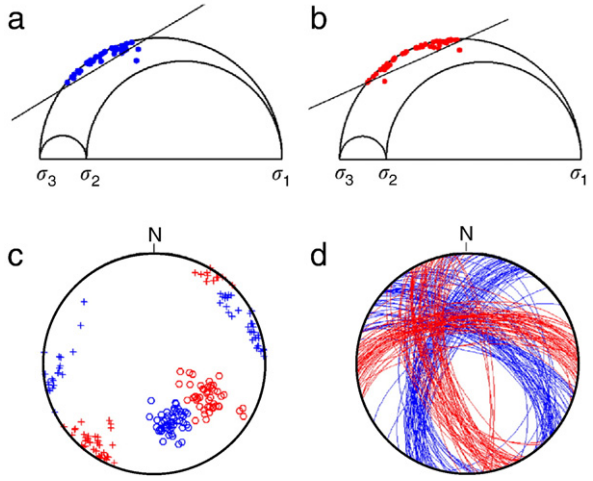

Fig. 9. Mohr's diagrams for separate clusters of the right-lateral (a) and left-lateral (b) faults. The P/T axes (c) and the nodal lines (d) for the right-lateral (in blue) and left-lateral (in red) focal mechanisms. The P and T axes in (c) are marked by open circles and plus signs, respectively.

differences in their friction. Fig. 9 indicates that the friction might be slightly different if retrieved from the cluster of the right-lateral or left-lateral faults only. The left-lateral faults are characterized by friction of 0.45, while the right-lateral faults by friction of 0.60. However, this difference is not very obvious and should be verified on more extensive datasets.

The tectonic and seismicity map immediately indicates that the principal faults play an essential role in the region (Fig. 10). The micro-earthquakes occur mostly on the left-lateral strike-slip principal fault with a strike of 169°. More than 90% of the events in the 2008 earthquake swarm were related to this fault. The orientation of this fault was independently determined also from the clustering of hypocentres (Fischer et al., 2010). This fault was active also during previous earthquake swarms, e.g., in 1985/86 (Vavryčuk, 1993) and in 2000 (Fischer, 2003; Fischer and Horálek, 2003). Interestingly, this fault has little geological expression on the Earth's surface. On the contrary, the right-lateral strike-slip principal fault with strike of 304° is less active at present. However, the system of faults of this orientation (Bankwitz et al., 2003; Zang and Stephansson, 2010) is well manifested on the Earth's surface in the focal area (Fig. 10). The unbalanced activity along both principal faults is probably caused by slightly different friction or may reflect the current distribution of pore pressure with the higher pressure localized within the left-lateral strike-slip principal fault.

5. Discussion and conclusions

The theoretical stress analysis and observations in West Bohemia provide evidence that activated faults should be similar to principal faults. It points to a long-term interaction of stress with fracturing of a structure. The medium is repeatedly fractured during its tectonic history along a variety of diversely oriented faults. Stress can create new optimally oriented fractures and heal the other misoriented fractures. Hence, the gradual evolution of fractures in rocks under stress probably has a tendency to develop, conserve and activate predominantly principal fractures and faults. Obviously, this statement is valid in a statistical sense only and does not exclude the reactivation of more misoriented faults, provided they are rather mature and weak (Sibson, 1990, 2007; Sibson and Xie, 1998).

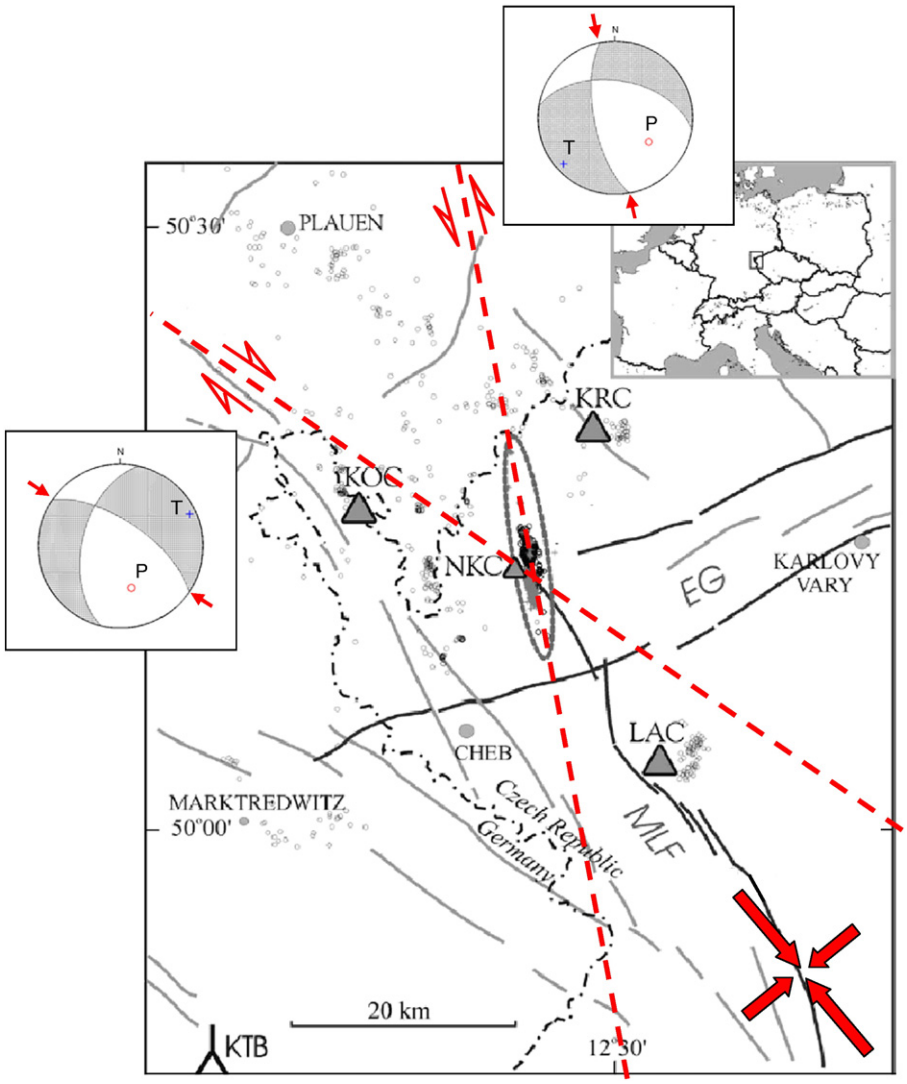

Fig. 10. Tectonic sketch of the West Bohemia/Vogtland region (modified after [Fischer, 2003]). The main fault systems are denoted as MLF (Mariánské-Lázně fault) and EG (Eger Rift). The grey dots mark the epicentres of micro-earthquakes that occurred in 1991–1999. The 2000 and 2008 swarm epicentres are inside the ellipse, which delineates the most active focal zone in the area (the Nový Kostel zone). The red dashed lines show the orientation of the principal faults found from stress analysis. The full red arrows show the orientation of maximum and minimum compressive stress axes. The two focal mechanisms correspond to the principal faults, the principal fault nodal lines are marked by red arrows. The black dashed-dotted line shows the border between the Czech Republic and Germany. KTB denotes the location of the KTB superdeep borehole.

In inverting the stress from focal mechanisms, it is necessary to find and select focal mechanisms corresponding to both conjugate principal faults. The principal faults need not be the major faults in the region, and the principal earthquakes need not coincide with the strongest earthquakes. A proper dataset of focal mechanisms suitable for stress inversion must cover the whole variety of focal mechanisms in the region homogeneously. If the distribution is unbalanced and the input focal mechanisms correspond prevailingly to only one principal fault, the stress inversion may yield biased results. If the distribution is properly balanced and the focal mechanisms are accurate we can map the butterfly wing pattern of the P/T axes. Subsequently, we can deduce an accurate stress orientation and reliable values of the shape ratio and fault friction.

It should be emphasized that diversity in focal mechanisms is inherent under any stress regime and does not necessarily imply a heterogeneous stress. The diversity originates in the existence of two conjugate sets of focal mechanisms and in the butterfly wing pattern of the P/T axes. If the focal mechanisms of both types occur subsequently in time then one can easily misinterpret this effect as a temporal variation of the stress orientation.

The distribution of nodal lines and compact clustering of the P/T axes of selected highly accurate focal mechanisms of the micro-earthquakes in the West Bohemia region indicates that tectonic stress is homogeneous in the focal area. This is particularly interesting taking into account that the magnitudes of the analyzed earthquakes range from 1 to 4. The local homogeneity of stress orientation is observed also in other areas (Hardebeck, 2006) and contradicts the idea that focal mechanisms of micro-earthquakes of low magnitudes should display a high scatter reflecting small scale stress heterogeneities (Rivera and Kanamori, 2002).

The most reliable method of determining the actual failure criterion and fault strength in a seismically active region is probably mapping active fault planes in the Mohr's diagram using extensive datasets of accurate focal mechanisms. According to this method, the average friction of active faults in West Bohemia is estimated to be 0.5. However, data indicate that the left-lateral strike-slip principal fault has a slightly lower value than the right-lateral. A lower value of friction can point to a more mature fault system and might be one of the reasons for higher seismic activity along this fault.

Acknowledgements

I thank two anonymous reviewers for detailed and constructive reviews, Pavla Hrubcová for help with preparing Fig. 6 and for many fruitful discussions of the topic, and Alena Boušková, Tomáš Fischer and Josef Horálek for providing me the data from the Webnet network and for help with their processing. The work was supported by the Grant Agency of the Academy of Sciences of the Czech Republic, Grant No. IAA300120801, by the Grant Agency of the Czech Republic, Grant No. P210/10/2063, and by the European Community's FP7 Consortium Project AIM “Advanced Industrial Microseismic Monitoring”, Grant Agreement No. 230669.

References

Angelier, J., 2002. Inversion of earthquake focal mechanisms to obtain the seismotectonic stress IV — a new method free of choice among nodal lines. Geophys. J. Int. 150, 568–609.
Babuška, V., Plomerová, J., Fischer, T., 2007. Intraplate seismicity in the western Bohemian Massif (central Europe): a possible correlation with a paleoplate junction. J. Geodyn. 44, 149–159.
Bankwitz, P., Schneider, G., Kämpf, H., Bankwitz, E., 2003. Structural characteristics of epicentral areas in Central Europe: study case Cheb Basin (Czech Republic). J. Geodyn. 35, 5–32.
Beeler, N.M., Simpson, R.W., Hickman, S.H., Lockner, D.A., 2000. Pore fluid pressure, apparent friction, and Coulomb failure. J. Geophys. Res. 105, 25.533–25.542.
Brudy, M., Zoback, M.D., Fuchs, K., Rummel, F., Baumgärtner, J., 1997. Estimation of the complete stress tensor to 8 km depth in the KTB scientific drill holes: implications for crustal strength. J. Geophys. Res. 102, 18 453–18 475.
Byerlee, J., 1978. Fiction of rocks. Pure Appl. Geophys. 116, 615–626.
Červený, V., 2001. Seismic Ray Theory. Cambridge University Press, Cambridge.
Fischer, T., 2003. The August–December 2000 earthquake swarm in NW Bohemia: the first results based on automatic processing of seismograms. J. Geodyn. 35, 59–81.
Fischer, T., Horálek, J., 2003. Space-time distribution of earthquake swarms in the principal focal zone of the NW Bohemia/Vogtland seismoactive region: period 1985–2001. J. Geodyn. 35, 125–144.
Fischer, T., Horálek, J., Michálek, J., Boušková, A., 2010. The 2008 West Bohemia earthquake swarm in the light of the WEBNET network. J. Seismolog. 14, 665–682.
Gephart, J.W., Forsyth, D.W., 1984. An improved method for determining the regional stress tensor using earthquake focal mechanism data: application to the San Fernando earthquake sequence. J. Geophys. Res. 89, 9305–9320.
Hardebeck, J.L., 2006. Homogeneity of small-scale earthquakes faulting, stress, and fault strength. Bull. Seismol. Soc. Am. 96, 1675–1688.
Hardebeck, J.L., Shearer, P.M., 2002. A new method for determining first-motion focal mechanisms. Bull. Seismol. Soc. Am. 92, 2264–2276.
Heidbach, O., Tingay, M., Barth, A., Reinecker, J., Kurfeß, D., Müller, B., 2008. The World Stress Map Database Release. doi:10.1594/GFZ.WSM.Rel2008.
Iio, Y., 1997. Frictional coefficient on faults in a seismogenic region inferred from earthquake mechanism solutions. J. Geophys. Res. 102 (B3), 5403–5412.
Jaeger, J.C., Cook, N.G.W., 1979. Fundamentals of Rock Mechanics. Chapman and Hall, New York.
Lund, B., Slunga, R., 1999. Stress tensor inversion using detailed microearthquake information and stability constraints: application to Ölfus in southwest Iceland. J. Geophys. Res. 104, 14 947–14 964.
Mavko, G., Mukerji, T., Dvorkin, J., 2009. The Rock Physics Handbook. Cambridge University Press.
Michael, A.J., 1984. Determination of stress from slip data: faults and folds. J. Geophys. Res. 89, 11,517–11,526 9.
Müller, B., Zoback, M.L., Fuchs, K., Mastin, L., Gregersen, S., Pavoni, N., Stephansson, O., Ljunggren, C., 1992. Regional patterns of tectonic stress in Europe. J. Geophys. Res. 97, 11 783–11 803.
Rivera, L., Kanamori, H., 2002. Spatial heterogeneity of tectonic stress and friction in the crust. Geophys. Res. Lett. 29. doi:10.1029/2001GL013803.
Scholtz, C.H., 2002. The Mechanics of Earthquakes and Faulting. Cambridge University Press, Cambridge.
Sibson, R.H., 1990. Rupture nucleation on unfavourably oriented faults. Bull. Seismol. Soc. Am. 80, 1580–1604.
Sibson, R.H., 2007. An episode of fault-valve behaviour during compressional inversion? — the 2004 M_J6.8 Mid-Niigata Prefecture, Japan, earthquake sequence. Earth Planet. Sci. Lett. 257, 188–199.
Sibson, R.H., Xie, G., 1998. Dip range for intracontinental reverse fault ruptures: Truth not stranger than friction? Bull. Seismol. Soc. Am. 88, 1014–1022.
Šílený, J., 2009. Resolution of non-double-couple mechanisms: simulation of hypocenter mislocation and velocity structure mismodelling. Bull. Seismol. Soc. Am. 99, 2265–2272.
Vavryčuk, V., 1993. Crustal anisotropy from local observations of shear-wave splitting in West Bohemia, Czech Republic. Bull. Seismol. Soc. Am. 83, 1420–1441.
Vavryčuk, V., 2002. Non-double-couple earthquakes of January 1997 in West Bohemia, Czech Republic: evidence of tensile faulting. Geophys. J. Int. 149, 364–373. doi:10.1046/j.1365-246X.2002.01654.x.
Zang, A., Stephansson, O., 2010. Stress Field of the Earth's Crust. Springer, New York.
Zoback, M.D., 2010. Reservoir Geomechanics. Cambridge University Press, Cambridge.